ACS APPLIED MATERIALS & INTERFACES

Research Article

Cite This: ACS Appl. Mater. Interfaces 2019, 11, 11834−11840

www.acsami.org

CdTe QD−CeO_2 Complex as a Strong Photoelectrochemical Signal Indicator for the Ultrasensitive microRNA Assay

Mengjie Li, Wenbin Liang, Ruo Yuan,* and Yaqin Chai*

Key Laboratory of Luminescent and Real-Time Analytical Chemistry (Southwest University), Ministry of Education, College of Chemistry and Chemical Engineering, Southwest University, Chongqing 400715, PR China

Supporting Information

ABSTRACT: The photoelectrochemical (PEC) signal can be enhanced by constructing sensitization structures containing photoactive materials and appropriate sensitizers. However, usually, the photoactive materials and sensitizers were separated in independent nanostructures, thereby producing long electron-transfer path and large energy loss, which could further result in limited photoelectric conversion efficiency and PEC signals. Herein, we designed a novel sensitization nanostructure simultaneously containing the photoactive material cerium dioxide (CeO_2) and its sensitizer CdTe quantum dots (QDs) as the strong PEC signal indicator (CdTe QD−CeO_2 complex), which prominently enhanced photoelectric conversion efficiency because of the shortened electron-transfer path and reduced energy loss. The proposed CdTe QD−CeO_2 complex was used to construct a PEC biosensor for achieving ultrasensitive determination of microRNA-141 (miRNA-141) coupling with target converting amplification and DNA supersandwich structure amplification. The designed PEC biosensor demonstrated a wide linear range from 0.5 fM to 5 nM with a detection limit of 0.17 fM for miRNA-141. Impressively, this work provided a new and strong PEC signal indicator for the construction of PEC sensing platform and would extend the application of PEC sensors in bioanalysis and early disease diagnosis.

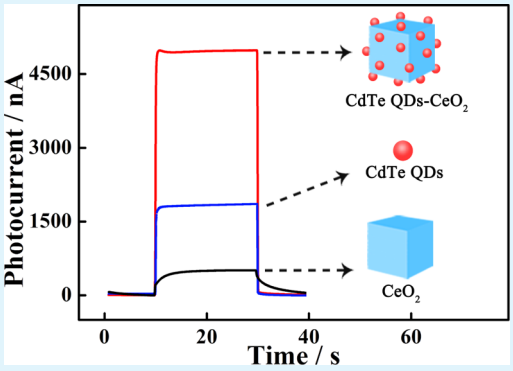

KEYWORDS: *photoelectrochemical sensing, CdTe QD−CeO_2 complex, signal indicator, dual signal amplification, microRNA assay*

INTRODUCTION

Photoelectrochemical (PEC) analysis, as a newly budding and exceedingly promising analytical method, employs light as the excitation source and current as the detection readout, and thus, it presents superior features of high sensitivity, reduced background noise, and excellent stability compared with conventional optical and electrochemical methods.[1−5] In recent years, great effort has been made on constructing sensitization structures containing photoactive materials and appropriate sensitizers to promote light-harvesting capability, enhance charge carrier separation, and depress electron−hole recombination, thereby improving the photoelectric conversion efficiency prominently.[6−10] For instance, Ju and Wen reported an efficient sensitization structure of CdTe quantum dots (QDs)/CdS QDs/TiO_2 nanoparticles for the construction of a protein detection platform.[8] Zhu and co-workers have proposed a PEC immunosensing platform for ultrasensitive carcinoembryonic antigen detection based on CdSeTe@CdS:Mn core−shell QD-sensitized TiO_2 nanoparticles.[9] Although these works can increase the photoelectric conversion efficiency to some extent, the PEC signals are still restricted because the photoactive materials and sensitizers are separated in independent nanostructures, leading to long electron-transfer path and large energy loss. Thus, it is expected to control the photoactive material and sensitizer within one nanostructure, which may greatly shorten electron-transfer path and reduce energy loss, thus further enhancing the photoelectric conversion efficiency and the PEC signal considerably.

Cerium dioxide (CeO_2), an attractive and typical semiconductor metal oxide, has been proverbially applied in the fields of catalysis, UV blocking, and PEC water splitting because of its advantages of steady physical and chemical properties as well as excellent photocatalytic activity.[11−13] Nevertheless, CeO_2 was rarely used in PEC sensing field owing to its wide band gap of 2.5 eV,[14] which seriously restricted the photoelectric conversion efficiency. This limitation might be lifted by combining the wide band gap CeO_2 and a narrower band gap semiconductor to construct an efficient sensitization structure. As a classic inorganic semiconductor, CdTe QDs possess ideal characteristics, such as tunable size, broad excitation, and high light-harvesting capability.[15−18] More importantly, the band gap of CdTe QDs is 1.8 eV,[19] which matches well with that of CeO_2 (2.5 eV), making CdTe QDs a promising sensitizer toward CeO_2. Considering these challenges and opportunities, we here attempted to synthesize a

Received: February 1, 2019
Accepted: March 11, 2019
Published: March 11, 2019

DOI: 10.1021/acsami.9b02189
ACS Appl. Mater. Interfaces 2019, 11, 11834−11840

Scheme 1. Schematic Diagrams of the Proposed PEC Biosensor for miRNA-141 Detection; (A) Preparation of the CdTe QD−CeO_2 Complex; (B) Target Converting Amplification Procedure

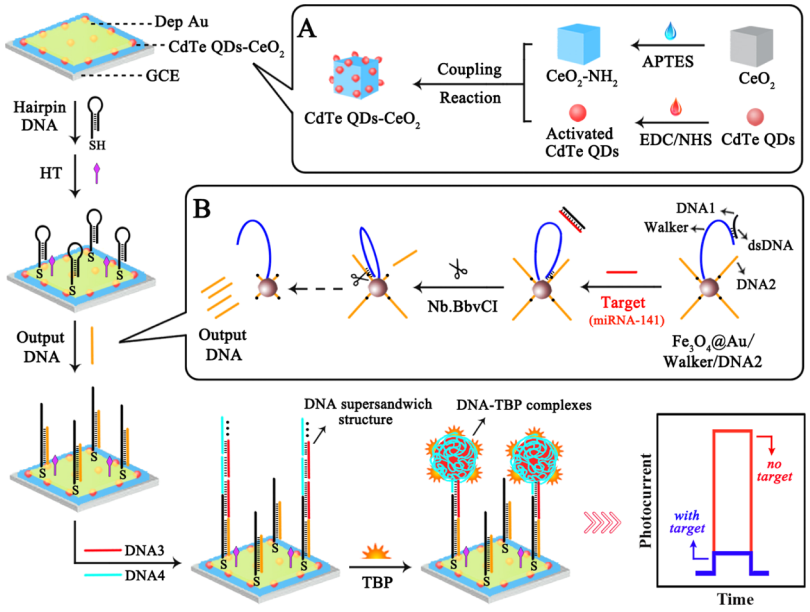

novel CdTe QD−CeO_2 complex by cross-linking $-NH_2$-functionalized CeO_2 and 3-mercaptopropionic acid (MPA)-capped CdTe QDs, in which the photoactive material CeO_2 and its sensitizer CdTe QDs were controlled in one nanostructure. In consequence, the CdTe QD−CeO_2 complex exhibited excellent photoelectric performances and could be employed as a strong PEC signal indicator, which was ascribed to the fact that CeO_2 and CdTe QDs were controlled in one nanostructure, leading to shortened electron-transfer path, reduced energy loss, and improved photoelectric conversion efficiency.

Herein, a PEC biosensor with the CdTe QD−CeO_2 complex as the PEC signal indicator was designed for ultrasensitive determination of miRNA-141 coupling with dual signal amplification strategy (Scheme 1). The successful synthesis of the CdTe QD−CeO_2 complex as a signal indicator could shorten the electron-transfer path and reduce the energy loss between CeO_2 and its sensitizer CdTe QDs, producing a strong PEC signal. Besides, the target converting amplification procedure based on DNA walker was adopted for achieving the conversion of small amounts of miRNA-141 to massive output DNA. These output DNAs could open hairpin DNA on the electrode surface and then trigger the generation of a DNA supersandwich structure containing numerous TATA sequences by the assistance of DNA3 and DNA4. With the addition of TATA-binding protein (TBP), the generated DNA supersandwich structure would specifically bind with TBP and bend at an 80° angle to form DNA−protein complexes,[20−24] which could effectively hinder the electron transfer, leading to a significantly reduced PEC signal for quantitative detection of miRNA-141. As expected, this work not only demonstrated the enormous potential of the CdTe QD−CeO_2 complex as a strong PEC signal indicator for sensing platform construction but also paved a new pathway for ultrasensitive detection of miRNA-141 in bioanalysis and early disease diagnosis.

EXPERIMENTAL SECTION

Synthesis of Fe_3O_4@Au, CdTe QDs, CeO_2, and CdTe QD−CeO_2 Complex. Fe_3O_4@Au and MPA-capped CdTe QDs were prepared based on the protocols reported previously.[25,26] CeO_2 was prepared using the method mentioned in the literature.[14,27] Briefly, 0.87 g of $Ce(NO_3)_3{\cdot}6H_2O$ was added to 40 mL of 6 M NaOH aqueous solution. After stirring for 0.5 h, the mixture was transferred into a 50 mL Teflon bottle and reacted at 180 °C for 24 h. After washing with ultrapure water until pH = 7, the precipitate was dried at 60 °C for 14 h and then calcined at 450 °C for 3 h. The obtained CeO_2 was stored at 4 °C prior to the $-NH_2$ functionalization. For the preparation of $-NH_2$-functionalized CeO_2 (CeO_2-NH_2), 2 mL of 3-aminopropyl triethoxysilane was dispersed in 20 mL of ethanol under stirring, followed by adjusting the pH to 5−8 with 3 M HCl. After that, 0.5 g of the as-prepared CeO_2 was added with constant stirring for 14 h. Finally, CeO_2-NH_2 was acquired by centrifugal washing.

For the preparation of the CdTe QD−CeO_2 complex, the amide reaction was adopted to link MPA-capped CdTe QDs and CeO_2-NH_2. First, 4 mL of 1-ethyl-3-(3-dimethylaminopropyl)carbodiimide/*N*-hydroxysuccinimide (10 mM/20 mM) solution was mixed with 2 mL of MPA-capped CdTe QDs for activation of −COOH groups. After washing by centrifugation, the activated MPA-capped CdTe QD was redispersed in 2 mL of ultrapure water, followed by adding 2 mL of CeO_2-NH_2 aqueous solution for 2 h. Finally, the CdTe QD−CeO_2 complex was collected through centrifugation and washing.

Target Converting Amplification Procedure. The target converting amplification procedure based on DNA walker is illustrated in Scheme 1B. First, 2 μL of 2 μM DNA1 was mixed with 2 μL of 2 μM thiolated walker at 37 °C for 2 h to form a double-stranded DNA (dsDNA). Next, the dsDNA and 40 μL of 2 μM thiolated DNA2 were simultaneously added into 40 μL of Fe_3O_4@Au with stirring for 14 h, thus obtaining the Fe_3O_4@Au/walker/DNA1/DNA2 complex through Au−S bond. Afterward, 2 μL of miRNA-141 (target) was added for realizing hybridization with DNA1 and releasing walker *via* a toehold exchange mechanism. The released walker paired with DNA2 on the surface of Fe_3O_4@Au, leading to the generation of a cleavage site for nicking endonuclease (Nb.BbvCI). In the presence of 2 μL of 5 U Nb.BbvCI and 4 μL of NE buffer, DNA2 would be cut by Nb.BvCI, producing output DNA. Simultaneously, walker would be released again for pairing with the next DNA2, which could achieve a further cutting and releasing process. In this way,

DOI: 10.1021/acsami.9b02189
ACS Appl. Mater. Interfaces 2019, 11, 11834−11840

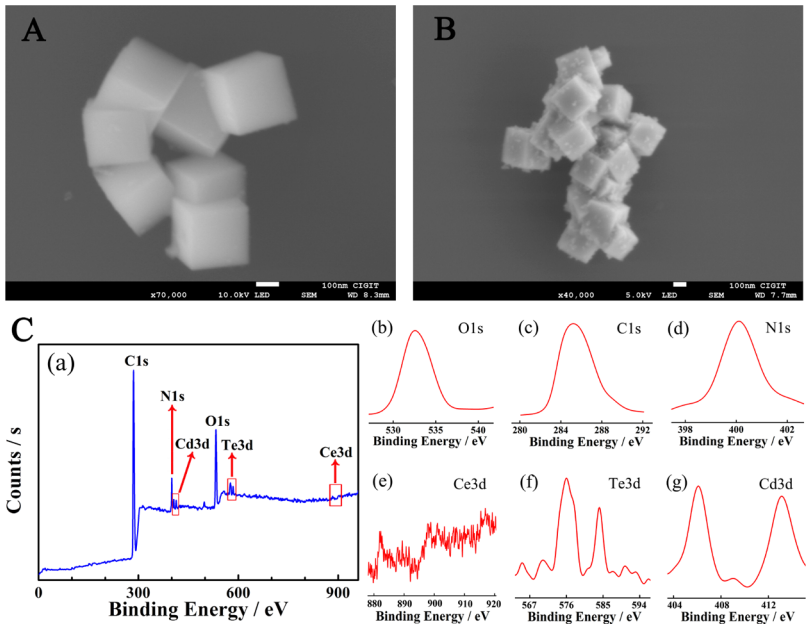

Figure 1. SEM images of (A) CeO_2 and (B) CdTe QD−CeO_2 complex. (C) XPS analysis of the (a) full region of the CdTe QD−CeO_2 complex, (b) O 1s region, (c) C 1s region, (d) N 1s region, (e) Ce 3d region, (f) Te 3d region, and (g) Cd 3d region.

numerous output DNA would be acquired *via* magnetic force and employed for opening hairpin DNA on the electrode surface.

Fabrication of the PEC Biosensor. After being cleaned according to the method reported previously,[28] the glassy carbon electrode (GCE) was decorated with 15 μL of the CdTe QD−CeO_2 complex and then dried at 37 °C. Next, the CdTe QD−CeO_2-modified GCE was immersed in 1% $HAuCl_4$ solution for 10 s to acquire a gold nanoparticle layer by electrodepositing under −0.2 V constant potential (DepAu), followed by dropping hairpin DNA (15 μL, 2 μM) and reacting for 14 h at 4 °C. After incubating hexanethiol (HT, 10 μL, 0.1 mM) for 0.5 h, 15 μL of output DNA was dropped on the electrode surface to hybridize with hairpin DNA. Subsequently, a DNA supersandwich structure was produced by adding DNA3 (10 μL, 2 μM) and DNA4 (10 μL, 2 μM), which possessed numerous TATA sequences and could specifically recognize TBP. Ultimately, the acquired electrode was incubated with 20 μL of 1 ng/mL TBP for 1 h to bend DNA at an 80° angle through the specific recognition between TBP and TATA sequences to form DNA−protein complexes. Scheme 1 presents the fabrication procedure of the PEC biosensor.

RESULTS AND DISCUSSION

Characterizations of Nanomaterials. The morphologies of CeO_2 and the CdTe QD−CeO_2 complex were investigated *via* scanning electron microscopy (SEM). Figure 1A is the SEM image of CeO_2, which presents a cubic structure with a uniform size of 250 nm. After reacting with CdTe QDs, as exhibited in Figure 1B, numerous CdTe QDs could be obviously observed on the surface of CeO_2 nanocubes. Furthermore, in order to confirm the successful synthesis of the CdTe QD−CeO_2 complex, the elemental analysis was obtained from the X-ray photoelectron spectroscopy (XPS). As illustrated in Figure 1C, XPS signals of O 1s, C 1s, and N 1s were found at binding energies of around 531.7, 284.8, and 399.4 eV, respectively, which demonstrated the presence of O, C, and N elements. These results were consistent with previous reports on O 1s, C 1s, and N 1s.[14,29] The Ce 3d binding energy peaks were investigated in detail in Figure S4 (Supporting Information). The peak was fitted into two peaks labeled as u″ and v′ to Ce^{3+}, and the other six peaks labeled as u, u′, u‴, v, v″, and v‴ to Ce^{4+}, which tallied with the literature data.[14,27] Besides, the doublets located at 576 and 584 eV belonged to Te 3d (Te $3d_{5/2}$ and Te $3d_{3/2}$), and two obvious peaks centered at 406 and 413 eV corresponded to Cd 3d (Cd $3d_{5/2}$ and Cd $3d_{3/2}$), which tallied with the previous report[30] and implied the existence of CdTe QDs. These results revealed that CeO_2 and the CdTe QD−CeO_2 complex were prepared successfully. Moreover, the characteristic results of the synthesized CdTe QDs and Fe_3O_4@Au are presented in Figure S3 (Supporting Information).

Gel Electrophoresis Analysis. As observed from Figure 2, the generation of a DNA supersandwich structure was characterized by polyacrylamide gel electrophoresis (PAGE). The result of hairpin DNA was shown in lane 1. Two bands could be obviously observed on lane 1 because the 3′-end of hairpin DNA was modified with thiol group and the formation of disulfide bond would lead to the increased molecular weight. Thus, the lower band on lane 1 represented hairpin DNA and the upper band on lane 1 indicated the formation of disulfide bonds. Compared with hairpin DNA (the lower band on lane 1), an increasing band shift was found from output DNA (lane 2) because of the reduced molecular weight. The result for hybridization of hairpin DNA with output DNA was shown in

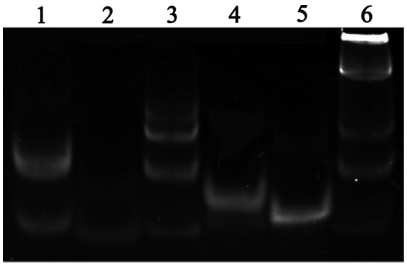

Figure 2. PAGE characterization: lane 1, hairpin DNA; lane 2, output DNA; lane 3, a mixture of hairpin DNA and output DNA; lane 4, DNA3; lane 5, DNA4; lane 6, a mixture of hairpin DNA, output DNA, DNA3, and DNA4.

DOI: 10.1021/acsami.9b02189
ACS Appl. Mater. Interfaces 2019, 11, 11834−11840

lane 3, which presented a slower band shift (lane 3 vs 1, 2), indicating that the hybridization between hairpin DNA and output DNA was successful. DNA3 (lane 4) and DNA4 (lane 5) with different molecular weights exhibited different band shifts. When hairpin DNA, output DNA, DNA3, and DNA4 coexisted (lane 6), output DNA could open hairpin DNA and then trigger the generation of DNA supersandwich structures, leading to the formation of a long dsDNA molecule. Accordingly, a band shift with the slowest mobility was found (lane 6), suggesting the successful generation of DNA supersandwich structures.

PEC Characterization of the Biosensor. As presented in Figure 3, PEC analysis was employed to characterize the modification process of this biosensor. The excitation light source with the wavelength of 460 nm and the radiant flux of 976 mW and the electrolyte solution of 5 mL phosphate-buffered solution (PBS) containing 0.1 M ascorbic acid (AA) were utilized during the PEC measurement. The PEC response of bare GCE was close to zero (curve a). After the CdTe QD−CeO_2 complex was modified on the surface of GCE, a greatly enhanced PEC response was observed (curve b) because of the excellent photoelectric activity of the CdTe QD−CeO_2 complex. Subsequent electrodeposition of gold nanoparticles caused a significantly increased PEC response (curve c) because of its excellent conductivity. The continuously decreased PEC responses were obtained (curves d−g) after successive assembly of hairpin DNA, nonconductive HT, output DNA, and DNA3−DNA4, owing to their poor charge transfer. Ultimately, a further decreased PEC response was found with the addition of TBP (curve h) because the electron-transfer path between the CdTe QD−CeO_2 complex and electron donor could be impeded by the produced DNA−TBP complexes. The result implied that the modification process of the PEC biosensor was successful.

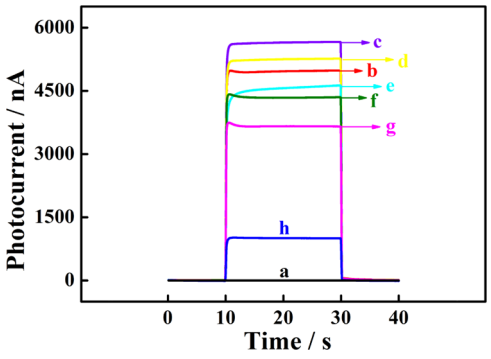

Figure 3. PEC responses of (a) bare GCE, (b) CdTe QD−CeO_2/GCE, (c) DepAu/CdTe QD−CeO_2/GCE, (d) hairpin DNA/DepAu/CdTe QD−CeO_2/GCE, (e) HT/hairpin DNA/DepAu/CdTe QD−CeO_2/GCE, (f) output DNA/HT/hairpin DNA/DepAu/CdTe QD−CeO_2/GCE, (g) DNA3−DNA4/output DNA/HT/hairpin DNA/DepAu/CdTe QD−CeO_2/GCE, and (h) TBP/DNA3−DNA4/output DNA/HT/hairpin DNA/DepAu/CdTe QD−CeO_2/GCE in PBS containing 0.1 M AA.

Comparison of Different Photoactive Materials. To explore the PEC efficiency of the CdTe QD−CeO_2 complex, two kinds of components including CeO_2 and CdTe QDs were selected for comparison under the same conditions. As illustrated in Figure 4, the PEC responses of CeO_2 and CdTe QDs were 505 and 1790 nA, respectively. A significantly enhanced PEC response (4980 nA) was obtained from the electrode surface modified with the CdTe QD−CeO_2 complex as the photoactive material (Figure 4C). In addition, the PEC responses of the CdTe QD−CeO_2 complex were 9.8-fold and 2.8-fold than those of pure CeO_2 and pure CdTe QDs, respectively. The key reasons for the PEC response enhancement were as follows: (a) the effective sensitization effect of CdTe QDs toward CeO_2 and (b) the prominently reduced electron-transfer distance between CeO_2 and CdTe QDs. The above results confirmed that the CdTe QD−CeO_2 complex with high PEC efficiency was a promising PEC signal indicator for application in PEC sensing platforms.

PEC Mechanism of the Biosensor. The PEC mechanisms of signal generating and quenching are shown in Figure 5. When the CdTe QD−CeO_2 complex was modified on the GCE surface, a strong PEC signal could be observed (Figure 5A), which might benefit from two reasons as follows. First, the effective band gap matching between CeO_2 and CdTe QDs could promote light-harvesting capability, facilitate charge separation, and depress electron−hole recombination, thus enhancing the photoelectric conversion efficiency. Second, CeO_2 and its sensitizer CdTe QDs controlled in one nanostructure could prominently reduce energy loss and enhance photoelectric conversion efficiency because of the shortened electron-transfer path. Concretely, under 460 nm illumination, electrons of CdTe QDs shifted from their valence band (VB) to their conduction band (CB) and then moved to the CB of CeO_2. Simultaneously, electrons of CeO_2 also shifted from their VB to their CB. These photogenerated electrons located at the CB of CeO_2 eventually migrated to GCE and the continuous electron supply from the electrolyte solution containing 0.1 M AA also occurred immediately, thus producing a strong PEC signal. Besides, the output DNA obtained from the target converting amplification procedure could trigger the generation of DNA supersandwich structures by the assistance of DNA3 and DNA4. The resulted DNA supersandwich structure containing numerous TATA sequences would specifically bind TBP and bend at an 80° angle to form DNA−protein complexes. Thereby, a great steric hindrance immediately produced and significantly hindered

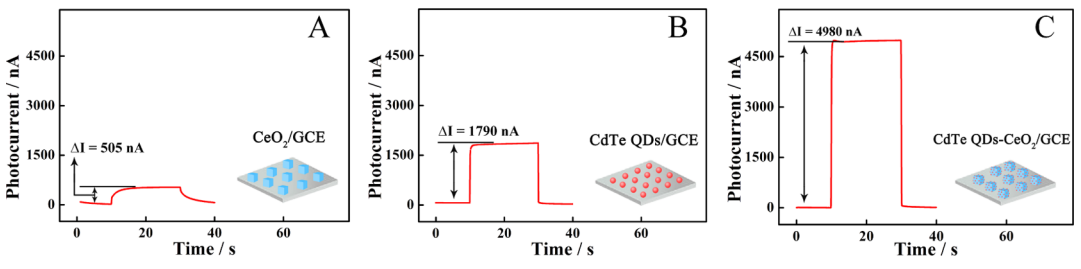

Figure 4. PEC responses of (A) CeO_2, (B) CdTe QDs, and (C) CdTe QD−CeO_2 complex in PBS containing 0.1 M AA.

DOI: 10.1021/acsami.9b02189
ACS Appl. Mater. Interfaces 2019, 11, 11834−11840

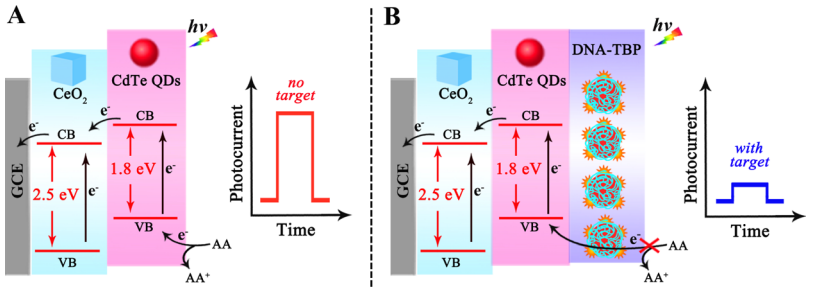

Figure 5. Mechanisms of (A) generation of PEC signal and (B) quenching of PEC signal.

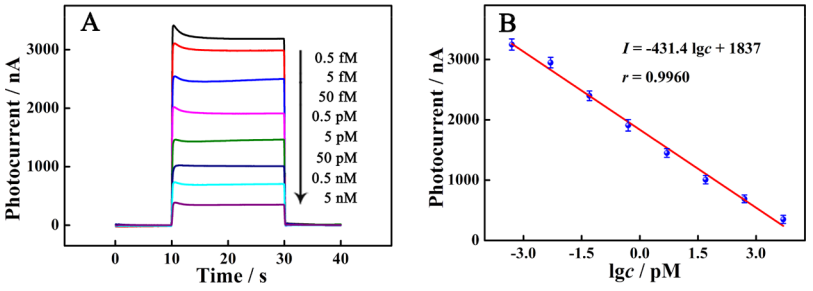

Figure 6. (A) PEC responses corresponding to different miRNA-141 levels. (B) Calibration curve for the miRNA-141 assay. Error bars represent standard deviations of three experiments.

the electron-transfer path between the CdTe QD−CeO_2 complex and electron donor (AA), resulting in a remarkably reduced PEC signal (Figure 5B).

Detection of miRNA-141. Under optimal conditions, the analytical characteristics of the developed biosensor were evaluated *via* quantitative detection of miRNA-141 with different concentrations. Figure 6A illustrated the PEC responses corresponding to different miRNA-141 levels, and the PEC response gradually decreased with the increasing miRNA-141 level from 0.5 fM to 5 nM. It could be obtained from Figure 6B that the PEC response was proportional to the logarithm of the miRNA-141 level, in which the linear equation was $I = -431.4 \lg c + 1837$ with $r = 0.9960$ (I: PEC response; c: miRNA-141 concentration; r: correlation coefficient). A detection limit of 0.17 fM was estimated based on the acknowledged calculation method,[31−33] and it was more sensitive compared with those of several published methodologies, which benefited from the introduction of dual signal amplification[34−36] and the efficient recognition of a detection probe to miRNA-141.[37,38] In addition, the specific comparison results for analytical characteristics between this developed biosensor and other assays reported previously are presented in Table 1.

Selectivity and Stability of the Proposed Biosensor. Selectivity and stability were two key indexes in measuring the PEC performances of this proposed biosensor. Possible interfering species, such as miRNA-21, miRNA-199a, and thrombin, were utilized for the assessment of selectivity. As observed from Figure 7A, the PEC signal for blank measurement presented no significant difference compared with 5 nM miRNA-21, 5 nM miRNA-199a, and 5 nM thrombin. However, when 50 pM miRNA-141 was employed for determination, an obviously reduced PEC signal was obtained. These consequences revealed a high selectivity of the PEC biosensor for miRNA-141 assay. Besides, under consecutive "off−on−off" light for 10 times, the time-based PEC signal toward 50 pM miRNA-141 was recorded (Figure 7B). The evident change of the PEC signal was not found with the light on, and the relative standard deviation was calculated as 0.92%, which implied that this biosensor possessed an excellent stability.

Table 1. Comparison of Different Methodologies for the miRNA Assay[a]

analytical method	detection limit	linear range	refs
fluorescence	10 fM	1 pM to 10 nM	39
electrochemistry	18 fM	50 fM to 500 nM	40
ECL	0.5 fM	1 fM to 1 nM	41
SPR	1 fM	0−50 pM	42
SERS	1 pM	1 pM to 100 nM	43
CL	10 fM	20 fM to 5 pM	44
PEC	153 fM	350 fM to 5 nM	45
PEC	83 fM	100 fM to 3 nM	46
PEC	0.31 pM	1 pM to 100 nM	34
PEC	0.17 fM	0.5 fM to 5 nM	our work

[a]Abbreviations: electrochemiluminescence (ECL); surface plasmon resonance (SPR); surface-enhanced Raman spectroscopy (SERS); chemiluminescence (CL).

CONCLUSIONS

In summary, a PEC biosensor with the CdTe QD−CeO_2 complex as the strong PEC signal indicator was successfully constructed for ultrasensitive assay of miRNA-141 coupling with dual signal amplification strategy. The proposed CdTe QD−CeO_2 complex possessed excellent photoelectric performances, and its PEC signal was 9.8-fold and 2.8-fold than those of pure CeO_2 and pure CdTe QDs, respectively, because the photoactive material CeO_2 and its sensitizer CdTe QDs were controlled in one nanostructure, leading to shortened electron-transfer path, reduced energy loss, and improved photoelectric conversion efficiency. Moreover, the introduction of dual signal amplification including target converting amplification and DNA supersandwich structure amplification

DOI: 10.1021/acsami.9b02189
ACS Appl. Mater. Interfaces 2019, 11, 11834−11840

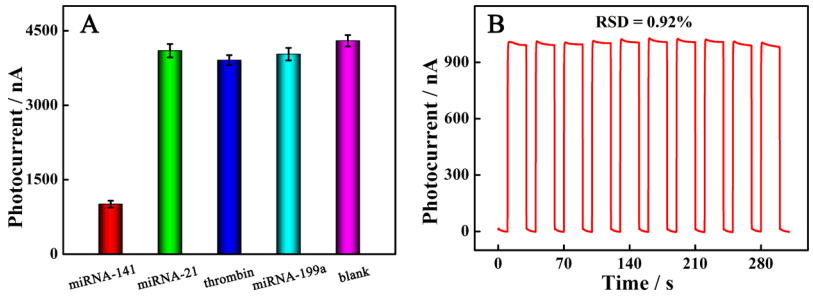

Figure 7. (A) Selectivity of the biosensor in the presence of different targets. (B) Stability of the biosensor. Error bars represent standard deviations of three experiments.

could effectively improve the detection sensitivity for miRNA-141 quantitative analysis. With the successful construction of the PEC sensing platform, this strategy not only offered a novel and promising PEC signal indicator but also revealed an efficient avenue for ultrasensitive miRNA estimation.

■ ASSOCIATED CONTENT

Supporting Information

The Supporting Information is available free of charge on the ACS Publications website at DOI: 10.1021/acsami.9b02189.

Materials and reagents, apparatus, gel electrophoresis, PEC measurement, condition optimization, electrochemical characterization of the PEC biosensor, characterizations of CdTe QDs and Fe_3O_4@Au, and XPS analysis of the Ce 3d region (PDF)

■ AUTHOR INFORMATION

Corresponding Authors

*E-mail: yuanruo@swu.edu.cn. Phone: +86-23-68252277. Fax: +86-23-68253172 (R.Y.).

*E-mail: yqchai@swu.edu.cn (Y.C.).

ORCID

Wenbin Liang: 0000-0002-9086-4974

Ruo Yuan: 0000-0003-3664-6236

Yaqin Chai: 0000-0003-4392-9592

Notes

The authors declare no competing financial interest.

■ ACKNOWLEDGMENTS

This work was financially supported by the NNSF of China (21575116, 21675129, and 21775124) and the Fundamental Research Funds for the Central Universities (XDJK2018AA003), China.

■ REFERENCES

(1) Zhao, W.-W.; Xu, J.-J.; Chen, H.-Y. Photoelectrochemical Immunoassays. *Anal. Chem.* **2018**, *90*, 615−627.

(2) Yang, R.; Yan, X.; Li, Y.; Zhang, X.; Chen, J. Nitrogen-Doped Porous Carbon-ZnO Nanopolyhedra Derived from ZIF-8: New Materials for Photoelectrochemical Biosensors. *ACS Appl. Mater. Interfaces* **2017**, *9*, 42482−42491.

(3) Li, L.; Zheng, X.; Huang, Y.; Zhang, L.; Cui, K.; Zhang, Y.; Yu, J. Addressable TiO_2 Nanotubes Functionalized Paper-Based Cyto-Sensor with Photocontrollable Switch for Highly-Efficient Evaluating Surface Protein Expressions of Cancer Cells. *Anal. Chem.* **2018**, *90*, 13882−13890.

(4) Dong, Y.-X.; Cao, J.-T.; Wang, B.; Ma, S.-H.; Liu, Y.-M. Spatial-Resolved Photoelectrochemical Biosensing Array Based on a CdS@g-C_3N_4 Heterojunction: A Universal Immunosensing Platform for Accurate Detection. *ACS Appl. Mater. Interfaces* **2018**, *10*, 3723−3731.

(5) Hao, Q.; Shan, X.; Lei, J.; Zang, Y.; Yang, Q.; Ju, H. A Wavelength-Resolved Ratiometric Photoelectrochemical Technique: Design and Sensing Applications. *Chem. Sci.* **2016**, *7*, 774−780.

(6) Song, Z.; Fan, G.-C.; Li, Z.; Gao, F.; Luo, X. Universal Design of Selectivity-Enhanced Photoelectrochemical Enzyme Sensor: Integrating Photoanode with Biocathode. *Anal. Chem.* **2018**, *90*, 10681−10687.

(7) An, T.; Tang, J.; Zhang, Y.; Quan, Y.; Gong, X.; Al-Enizi, A. M.; Elzatahry, A. A.; Zhang, L.; Zheng, G. Photoelectrochemical Conversion from Graphitic C_3N_4 Quantum Dot Decorated Semiconductor Nanowires. *ACS Appl. Mater. Interfaces* **2016**, *8*, 12772−12779.

(8) Wen, G.; Ju, H. Enhanced Photoelectrochemical Proximity Assay for Highly Selective Protein Detection in Biological Matrixes. *Anal. Chem.* **2016**, *88*, 8339−8345.

(9) Fan, G.-C.; Zhu, H.; Du, D.; Zhang, J.-R.; Zhu, J.-J.; Lin, Y. Enhanced Photoelectrochemical Immunosensing Platform Based on CdSeTe@CdS:Mn Core-Shell Quantum Dots-Sensitized TiO_2 Amplified by CuS Nanocrystals Conjugated Signal Antibodies. *Anal. Chem.* **2016**, *88*, 3392−3399.

(10) Wu, R.; Fan, G.-C.; Jiang, L.-P.; Zhu, J.-J. Peptide-Based Photoelectrochemical Cytosensor Using a Hollow-TiO_2/EG/$ZnIn_2S_4$ Co-sensitized Structure for Ultrasensitive Detection of Early Apoptotic Cells and Drug Evaluation. *ACS Appl. Mater. Interfaces* **2018**, *10*, 4429−4438.

(11) Su, J.; Xie, C.; Chen, C.; Yu, Y.; Kennedy, G.; Somorjai, G. A.; Yang, P. Insights into the Mechanism of Tandem Alkene Hydroformylation over a Nanostructured Catalyst with Multiple Interfaces. *J. Am. Chem. Soc.* **2016**, *138*, 11568−11574.

(12) Wang, X.; Li, X.; Liu, D.; Song, S.; Zhang, H. Green Synthesis of Pt/CeO_2/Graphene Hybrid Nanomaterials with Remarkably Enhanced Electrocatalytic Properties. *Chem. Commun.* **2012**, *48*, 2885−2887.

(13) Liu, J.-X.; Su, Y.; Filot, I. A. W.; Hensen, E. J. M. A Linear Scaling Relation for CO Oxidation on CeO_2-Supported Pd. *J. Am. Chem. Soc.* **2018**, *140*, 4580−4587.

(14) Zou, W.; Shao, Y.; Pu, Y.; Luo, Y.; Sun, J.; Ma, K.; Tang, C.; Gao, F.; Dong, L. Enhanced Visible Light Photocatalytic Hydrogen Evolution via Cubic CeO_2 Hybridized g-C_3N_4 Composite. *Appl. Catal., B* **2017**, *218*, 51−59.

(15) Zhang, L. B.; Jean, S. R.; Ahmed, S.; Aldridge, P. M.; Li, X. Y.; Fan, F. J.; Sargent, E. H.; Kelley, S. O. Multifunctional Quantum Dot DNA Hydrogels. *Nat. Commun.* **2017**, *8*, 381.

(16) Jasieniak, J.; Califano, M.; Watkins, S. E. Size-Dependent Valence and Conduction Band-Edge Energies of Semiconductor Nanocrystals. *ACS Nano* **2011**, *5*, 5888−5902.

(17) Crisp, R. W.; Pach, G. F.; Kurley, J. M.; France, R. M.; Reese, M. O.; Nanayakkara, S. U.; MacLeod, B. A.; Talapin, D. V.; Beard, M. C.; Luther, J. M. Tandem Solar Cells from Solution-Processed CdTe and PbS Quantum Dots Using a ZnTe-ZnO Tunnel Junction. *Nano Lett.* **2017**, *17*, 1020−1027.

DOI: 10.1021/acsami.9b02189
ACS Appl. Mater. Interfaces 2019, 11, 11834−11840

(18) Li, Q.; Xu, Z.; McBride, J. R.; Lian, T. Low Threshold Multiexciton Optical Gain in Colloidal CdSe/CdTe Core/Crown Type-II Nanoplatelet Heterostructures. *ACS Nano* **2017**, *11*, 2545−2553.
(19) Fan, G.-C.; Han, L.; Zhang, J.-R.; Zhu, J.-J. Enhanced Photoelectrochemical Strategy for Ultrasensitive DNA Detection Based on Two Different Sizes of CdTe Quantum Dots Cosensitized TiO_2/CdS:Mn Hybrid Structure. *Anal. Chem.* **2014**, *86*, 10877−10884.
(20) Patel, A. B.; Louder, R. K.; Greber, B. J.; Grünberg, S.; Luo, J.; Fang, J.; Liu, Y. T.; Ranish, J.; Hahn, S.; Nogales, E. Structure of Human TFIID and Mechanism of TBP Loading onto Promoter DNA. *Science* **2018**, *362*, No. eaau8872.
(21) Liu, N.; Yang, Z.; Lou, X.; Wei, B.; Zhang, J.; Gao, P.; Hou, R.; Xia, F. Nanopore-Based DNA-Probe Sequence-Evolution Method Unveiling Characteristics of Protein-DNA Binding Phenomena in a Nanoscale Confined Space. *Anal. Chem.* **2015**, *87*, 4037−4041.
(22) Ma, Z.-Y.; Ruan, Y.-F.; Xu, F.; Zhao, W.-W.; Xu, J.-J.; Chen, H.-Y. Protein Binding Bends the Gold Nanoparticle Capped DNA Sequence: Toward Novel Energy-Transfer-Based Photoelectrochemical Protein Detection. *Anal. Chem.* **2016**, *88*, 3864−3871.
(23) Ma, Z.-Y.; Ruan, Y.-F.; Zhang, N.; Zhao, W.-W.; Xu, J.-J.; Chen, H.-Y. A New Visible-Light-Driven Photoelectrochemical Biosensor for Probing DNA-Protein Interactions. *Chem. Commun.* **2015**, *51*, 8381−8384.
(24) Delgadillo, R. F.; Whittington, J. E.; Parkhurst, L. K.; Parkhurst, L. J. The TATA-Binding Protein Core Domain in Solution Variably Bends TATA Sequences via a Three-Step Binding Mechanism. *Biochemistry* **2009**, *48*, 1801.
(25) Li, M.-J.; Zheng, Y.-N.; Liang, W.-B.; Yuan, R.; Chai, Y.-Q. Using p-type PbS Quantum Dots to Quench Photocurrent of Fullerene-Au NP@MoS_2 Composite Structure for Ultrasensitive Photoelectrochemical Detection of ATP. *ACS Appl. Mater. Interfaces* **2017**, *9*, 42111−42120.
(26) Li, M.; Zheng, Y.; Liang, W.; Yuan, Y.; Chai, Y.; Yuan, R. An Ultrasensitive "on−off−on" Photoelectrochemical Aptasensor Based on Signal Amplification of a Fullerene/CdTe Quantum Dots Sensitized Structure and Efficient Quenching by Manganese Porphyrin. *Chem. Commun.* **2016**, *52*, 8138−8141.
(27) Zou, W.; Ge, C.; Lu, M.; Wu, S.; Wang, Y.; Sun, J.; Pu, Y.; Tang, C.; Gao, F.; Dong, L. Engineering the NiO/CeO_2 Interface to Enhance the Catalytic Performance for CO Oxidation. *RSC Adv.* **2015**, *5*, 98335−98343.
(28) Zhang, P.; Jiang, J.; Yuan, R.; Zhuo, Y.; Chai, Y. Highly Ordered and Field-Free 3D DNA Nanostructure: The Next Generation of DNA Nanomachine for Rapid Single-Step Sensing. *J. Am. Chem. Soc.* **2018**, *140*, 9361−9364.
(29) Zhen, J.; Liu, Q.; Chen, X.; Li, D.; Qiao, Q.; Lu, Y.; Yang, S. An Ethanolamine-Functionalized Fullerene as an Efficient Electron Transport Layer for High-Efficiency Inverted Polymer Solar Cells. *J. Mater. Chem. A* **2016**, *4*, 8072−8079.
(30) He, Y.; Lu, H.-T.; Sai, L.-M.; Su, Y.-Y.; Hu, M.; Fan, C.-H.; Huang, W.; Wang, L.-H. Microwave Synthesis of Water-Dispersed CdTe/CdS/ZnS Core-Shell-Shell Quantum Dots with Excellent Photostability and Biocompatibility. *Adv. Mater.* **2008**, *20*, 3416−3421.
(31) He, L.; Lu, D.-Q.; Liang, H.; Xie, S.; Luo, C.; Hu, M.; Xu, L.; Zhang, X.; Tan, W. Fluorescence Resonance Energy Transfer-Based DNA Tetrahedron Nanotweezer for Highly Reliable Detection of Tumor-Related mRNA in Living Cells. *ACS Nano* **2017**, *11*, 4060−4066.
(32) Radi, A.-E.; Acero Sánchez, J. L.; Baldrich, E.; O'Sullivan, C. K. Reagentless, Reusable, Ultrasensitive Electrochemical Molecular Beacon Aptasensor. *J. Am. Chem. Soc.* **2006**, *128*, 117−124.
(33) Qu, X.; Xiao, M.; Li, F.; Lai, W.; Li, L.; Zhou, Y.; Lin, C.; Li, Q.; Ge, Z.; Wen, Y.; Pei, H.; Liu, G. Framework Nucleic Acid-Mediated Pull-Down MicroRNA Detection with Hybridization Chain Reaction Amplification. *ACS Appl. Bio Mater.* **2018**, *1*, 859−864.
(34) Chu, Y.; Wu, R.; Fan, G.-C.; Deng, A.-P.; Zhu, J.-J. Enzyme-Free Photoelectrochemical Biosensor Based on the Co-Sensitization Effect Coupled with Dual Cascade Toehold-Mediated Strand Displacement Amplification for the Sensitive Detection of MicroRNA-21. *ACS Sustainable Chem. Eng.* **2018**, *6*, 11633−11641.
(35) Wang, Y.; Bai, J.; Huo, B.; Yuan, S.; Zhang, M.; Sun, X.; Peng, Y.; Li, S.; Wang, J.; Ning, B.; Gao, Z. Upconversion Fluorescent Aptasensor for Polychlorinated Biphenyls Detection Based on Nicking Endonuclease and Hybridization Chain Reaction Dual-Amplification Strategy. *Anal. Chem.* **2018**, *90*, 9936−9942.
(36) Ma, F.; Liu, W.-j.; Liang, L.; Tang, B.; Zhang, C.-Y. Sensitive Detection of Alkaline Phosphatase by Dephosphorylation-Initiated Transcription Reaction-Mediated Dual Signal Amplification. *Chem. Commun.* **2018**, *54*, 2413−2416.
(37) Qu, X.; Zhu, D.; Yao, G.; Su, S.; Chao, J.; Liu, H.; Zuo, X.; Wang, L.; Shi, J.; Wang, L.; Huang, W.; Pei, H.; Fan, C. An Exonuclease III-Powered, On-Particle Stochastic DNA Walker. *Angew. Chem., Int. Ed.* **2017**, *56*, 1855−1858.
(38) Ge, Z.; Lin, M.; Wang, P.; Pei, H.; Yan, J.; Shi, J.; Huang, Q.; He, D.; Fan, C.; Zuo, X. Hybridization Chain Reaction Amplification of MicroRNA Detection with a Tetrahedral DNA Nanostructure-Based Electrochemical Biosensor. *Anal. Chem.* **2014**, *86*, 2124−2130.
(39) Xiao, M.; Man, T.; Zhu, C.; Pei, H.; Shi, J.; Li, L.; Qu, X.; Shen, X.; Li, J. MoS_2 Nanoprobe for MicroRNA Quantification Based on Duplex-Specific Nuclease Signal Amplification. *ACS Appl. Mater. Interfaces* **2018**, *10*, 7852−7858.
(40) Jiang, J.; Lin, X.; Diao, G. Smart Combination of Cyclodextrin Polymer Host-Guest Recognition and Mg^{2+}-Assistant Cyclic Cleavage Reaction for Sensitive Electrochemical Assay of Nucleic Acids. *ACS Appl. Mater. Interfaces* **2017**, *9*, 36688−36694.
(41) Feng, Q.-M.; Shen, Y.-Z.; Li, M.-X.; Zhang, Z.-L.; Zhao, W.; Xu, J.-J.; Chen, H.-Y. Dual-Wavelength Electrochemiluminescence Ratiometry Based on Resonance Energy Transfer between Au Nanoparticles Functionalized g-C_3N_4 Nanosheet and $Ru(bpy)_3^{2+}$ for MicroRNA Detection. *Anal. Chem.* **2016**, *88*, 937−944.
(42) Wang, Q.; Li, Q.; Yang, X.; Wang, K.; Du, S.; Zhang, H.; Nie, Y. Graphene Oxide-Gold Nanoparticles Hybrids-based Surface Plasmon Resonance for Sensitive Detection of MicroRNA. *Biosens. Bioelectron.* **2016**, *77*, 1001−1007.
(43) Qi, L.; Xiao, M.; Wang, X.; Wang, C.; Wang, L.; Song, S.; Qu, X.; Li, L.; Shi, J.; Pei, H. DNA-Encoded Raman-Active Anisotropic Nanoparticles for MicroRNA Detection. *Anal. Chem.* **2017**, *89*, 9850−9856.
(44) Deng, H.; Ren, Y.; Shen, W.; Gao, Z. An Ultrasensitive Homogeneous Chemiluminescent Assay for MicroRNAs. *Chem. Commun.* **2013**, *49*, 9401−9403.
(45) Tu, W.; Cao, H.; Zhang, L.; Bao, J.; Liu, X.; Dai, Z. Dual Signal Amplification Using Gold Nanoparticles-Enhanced Zinc Selenide Nanoflakes and P19 Protein for Ultrasensitive Photoelectrochemical Biosensing of MicroRNA in Cell. *Anal. Chem.* **2016**, *88*, 10459−10465.
(46) Liu, S.; Cao, H.; Wang, X.; Tu, W.; Dai, Z. Green light excited ultrasensitive photoelectrochemical biosensing for microRNA at a low applied potential based on the dual role of Au NPs in TiO_2 nanorods/Au NPs composites. *Nanoscale* **2018**, *10*, 16474−16478.

DOI: 10.1021/acsami.9b02189
ACS Appl. Mater. Interfaces 2019, 11, 11834−11840